Dramatically Enhanced Mechanical Performance of Nylon-6 Magnetic Composites with Nanostructured Hybrid One-Dimensional Carbon Nanotube-Two-Dimensional Clay Nanoplatelet Heterostruc...

ARTICLE *in* THE JOURNAL OF PHYSICAL CHEMISTRY B · MARCH 2011

Impact Factor: 3.3 · DOI: 10.1021/jp112284k · Source: PubMed

6 AUTHORS, INCLUDING:

Chao Zhang
Donghua University
43 PUBLICATIONS **1,064** CITATIONS
SEE PROFILE

Tianxi Liu
Fudan University
232 PUBLICATIONS **7,166** CITATIONS
SEE PROFILE

In Yee Phang
Agency for Science, Technology and Researc...
62 PUBLICATIONS **2,406** CITATIONS
SEE PROFILE

THE JOURNAL OF PHYSICAL CHEMISTRY B

ARTICLE

pubs.acs.org/JPCB

Dramatically Enhanced Mechanical Performance of Nylon-6 Magnetic Composites with Nanostructured Hybrid One-Dimensional Carbon Nanotube−Two-Dimensional Clay Nanoplatelet Heterostructures

Chao Zhang,[†] Weng Weei Tjiu,[‡] Tianxi Liu,[*,†] Wai Yi Lui,[‡] In Yee Phang,[‡] and Wei-De Zhang[*,§]

[†]Key Laboratory of Molecular Engineering of Polymers of Ministry of Education, Department of Macromolecular Science, Fudan University, Shanghai 200433, P. R. China

[‡]Institute of Materials Research and Engineering, A*STAR (Agency for Science, Technology and Research), 3 Research Link, Singapore 117602

[§]Nano Science Research Center, School of Chemistry and Chemical Engineering, South China University of Technology, Guangzhou, 510640, P.R. China

ABSTRACT: Mechanically robust, magnetic nylon-6 nanocomposites reinforced by one-dimensional (1D) carbon nanotube (CNT)−two-dimensional (2D) clay nanoplatelet hybrids have been prepared using a simple melt-compounding technique. The direct iron-catalyzed chemical vapor deposition (CVD) growth of multiwalled CNTs utilizes iron oxide-immobilized clay nanoplatelets as substrates, carrying out in situ intercalation and exfoliation of clay nanoplatelets. By using such a hybridization and coexfoliation method, the as-obtained heterostructured hybrids used without any purification are demonstrated to be ideal and excellent nanofillers for mechanical reinforcement for fabricating nylon-6 nanocomposites, due to their homogeneous dispersion and strong interfacial interaction with the polymer matrix. The nucleation sites provided by the nanohybrids seem to be favorable to the formation of thermodynamically stable α-phase crystals of nylon-6 with much higher stiffness and hardness than γ-form of nylon-6, namely, a silicate-induced crystal transformation from the α-form to the γ-form of nylon-6 was greatly inhibited or "shielded" by the CNT-wrapped clay nanoplatelets. Furthermore, the nanostructured CNT−clay hybrid heterostructures containing residual iron oxide nanoparticles show novel magnetic properties in both bulk solids and polymer nanocomposites. Therefore, this can be probably developed into a facile and practical method to fabricate polymer nanocomposites with high performance and multifunctionality.

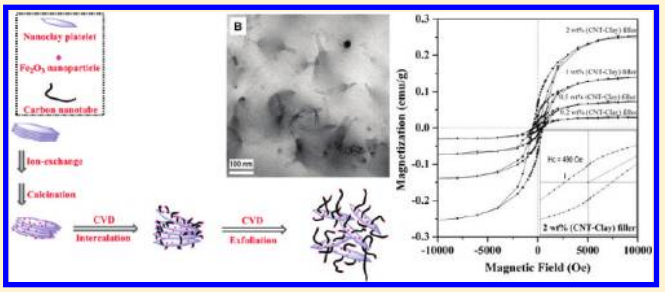

1. INTRODUCTION

The promising development of structural material with high strength, high modulus, high (or low) thermal resistance, and low density indicates that the contemporary research and development goals are pursuing composite structural material by incorporation with a variety of fillers in a matrix. In the past few years, nanomaterial reinforced plastics, rubber, and ceramic nanocomposites with high performance have drawn much attention from either academic or industrial circles, and are likely to not only bring high technology into traditional industries but also offer a cheaper and more environmentally friendly production route. Nanomaterials,[1] exhibiting exciting optical, electrical, and mechanical properties due to their size, have great challenges and opportunities for applications toward nanotechnology, biology, and catalysis.[2−5] In the realm of polymer nanocomposites reinforced by nanomaterials, in addition to increasing mechanical properties of the polymer matrix, making polymer composites with unique electrical, magnetic, and optical properties will become a new research highlight. Hybrid nanomaterials,[6−11] composed of two heterogeneous nanoelementary units with different properties, can be designed to prepare a new class of efficient, functional, multidimensional composite nanofillers. When being incorporated with polymers through different approaches such as simple melt compounding, these well-designed hybrid nanofillers can play an important role in fabricating high-performance and multifunctional polymer nanocomposites. Therefore, the next technological frontiers will be opened by designing and optimizing nanomaterial combinations and their synergistic functions. Additionally, it can be expected that the agglomeration of the nanoparticles and interfacial interaction problems in polymer nanocomposites could be solved simultaneously by using such functional hybrid nanofillers.

Currently, the most commonly used inorganic nanofillers for polymer composites are as follows: quasi one-dimensional (1D) single-walled and multiwalled carbon nanotubes (MWNTs), two-dimensional (2D) mica-type clay (such as montmorillonite),

Received: December 27, 2010
Revised: February 21, 2011
Published: March 15, 2011

and three-dimensional (3D) nanocalcium carbonate ($CaCO_3$), nanosilica (SiO_2), and so on. Among them, the most promising nanomaterials with excellent mechanical strength, electrical and thermal conductivity, and optical properties are carbon nanotubes (CNTs),[12−15] which have seen increased research focus due to their unique structural features since their discovery in 1991.[16] The advantages of CNTs, including their high aspect ratio (usually >1000), tubular geometry, large specific surface area, and percolation at very low volume fractions, determine its potential benefit as an ideal building block in the preparation of hybrid materials.[17] Over recent years, CNTs have been combined with a variety of inorganic compounds, including oxides, carbides, chalcogenides, and ceramics. Among these, the oxides have by far been the most commonly explored species. The hybridization of 1D CNTs and 2D lamellar flakes thus leading to 3D hybrid nanomaterials is crucial, as it can enable excellent performances and tailor-made properties compared with individual nanomaterials. For instance, combined 3D (clay−CNT) hybrid/polymer nanocomposites show extraordinary mechanical and energy-absorbing properties.[18−22] Similarly, a hierarchical composite of single/double-walled CNTs interlinked with 2D flakes can be constructed via in situ CNT growth onto layered double hydroxide (LDH) flakes and the hierarchical composite is demonstrated to be excellent fillers for preparing strong polyimide composite films.[23] Recently, CNTs were found to be easily dispersed in water assisted with graphene oxide,[24,25] which provide a clean and convenient method for preparing polymer nanocomposites in an aqeuous process.[26]

Nylon-6 is one of the most frequently used engineering plastics. Earlier studies have considered either nanoclay or CNTs as reinforcing fillers to fabricate high-performance nylon-6-based composites. Unfortunately, for ages researchers have not found the antidote to the problem of the full realization of the potential of nanoparticles as reinforcement for polymers due to the dispersion and interfacial interaction problems.[27] Wang et al.[28] functionalized MWNTs by sonication-induced in situ emulsion polymerization to obtain polymer-encapsulated CNTs. When melt compounded with nylon-6, they found that polymer-encapsulated CNTs could be well dispersed in a nylon-6 matrix, and the tensile strength and Young's modulus of composites were improved by 30% and 35%, respectively, by adding 1 wt % polymer-encapsulated CNTs. Previously, our group[29] also fabricated nylon-6/MWNT composites by a simple melt compounding method, and a homogeneous dispersion of MWNTs and strong interfacial adhesion between the MWNTs and nylon-6 matrix were successfully achieved. The yield strength and Young's modulus were increased by about 214% and 162%, respectively, at a loading level of 2 wt % MWNTs.

In this paper, we report an in situ CNT growth onto iron oxide-immobilized nanoclay platelets to directly form a 3D hierarchical hybrid nanostructure, nominated as CNT−clay hybrids. Simultaneously, intercalation and exfoliation of clay nanoplatelets were achieved due to the impetus of CNT growth within the clay interlayers. Moreover, the residual iron oxide catalyst endowed CNT−clay hybrids with novel magnetic properties. High-performance nylon-6/(CNT−clay hybrid) composites were thus fabricated from the as-grown products to show the extraordinary performance of the hierarchical composite of CNT−clay hybrids as reinforcing fillers. Different from silicate-induced crystal transformation from the α-form to the γ-form of nylon-6,[30−34] the nucleation sites provided by CNTs,[29,35] as well as the CNT−clay hybrids regarded as CNT-encapsulated or -covered clay nanoplatelets, were inclined to form thermodynamically stable α-phase crystals of nylon-6, showing more promising mechanical properties than the γ-phase crystals.

2. EXPERIMENTAL SECTION

2.1. Reagents and Materials. Sodium montmorillonite (Na^+MMT) was purchased from Southern Clay Products, Inc., Gonzales, TX. The nylon-6 pellets (Grade SF1080A) used in this study were the product of Ube Industries under license from Toyota. All the other reactants were purchased from Aldrich and used as received. Ultrapure Milli-Q water was used throughout all the experiments.

2.2. Preparation of CNT−Clay Hybrids. $Fe(NO_3)_3 \cdot 9H_2O$ (18 g) was dissolved in 100 mL of deionized (DI) water and stirred for 15 min at room temperature to dissolve the compound completely. Na^+MMT (10 g) was suspended in 150 mL of DI water, transferred into a 500 mL reaction flask, and then mixed with the $Fe(NO_3)_3$ solution. The mixture was stirred for at least 1 h below 30 °C, and then another 10 h under refluxing with intense stirring to synthesize the Fe^{3+}-intercalated MMT. The resulting solid obtained by evaporating the solvent was dried at 120 °C overnight and then calcined at 500 °C for 3 h. The obtained solid was ground and sieved to obtain particles smaller than 400 mesh (0.037 mm), which were used for the chemical vapor deposition (CVD) growth of CNTs. The Fe−clay catalyst obtained above contained about 20 wt % Fe. The CNTs were grown on the iron catalyst-immobilized clay by catalytic CVD with mixed gases containing 5 vol % acetylene diluted with nitrogen at 700 °C. The CNT content was about 40 wt % according to the weight of the catalyst after 10 min of reaction time.

2.3. Fabrication of Nylon-6/CNT−Clay Hybrid Composites. Nylon-6 composites containing different CNT−clay hybrid contents (from 0 to 2 wt %) were prepared via a melt-compounding method using a Brabender twin-screw mixer at 250 °C for 10 min with a screw speed of 100 rpm. Film samples (with thickness of about 0.5 mm) were prepared by compression molding in a press at a temperature of 250 °C with a pressure of 150 bar, followed by quick quenching in an ice/water bath.

2.4. Characterization. The prepared samples were characterized by wide-angle X-ray diffraction (WAXD; Bruker D8 GADDS), scanning electron microscopy (SEM; JEOL JSM 6700F), and transmission electron microscopy (TEM; Philips CM300 FEG TEM). The tensile tests were carried out using an Instron universal material testing system (model 5567) with dog-bone specimens (63.5 mm ×9.53 mm ×3.18 mm, Die ASTM D-638 Type V). Thermogravimetric analysis (TGA) was performed from 50 to 800 °C at a heating rate of 20 °C min^{-1} by using Q-500 (TA Instruments) under nitrogen atmosphere. Dynamic mechanical analysis (DMA) was performed on the samples of 30 × 10 × 0.5 mm^3 in size using a dynamic mechanical analyzer from TA Instruments under tension film mode in a temperature range of −135−200 °C at a frequency of 1 Hz and heating rate of 3 °C min^{-1}. DSC experiments were performed in a DSC-2920 from TA Instruments coupled with a TA-2000 control system. The samples were heated or cooled at a scanning rate of 10 °C min^{-1} under nitrogen atmosphere in order to diminish oxidation. The magnetic properties of the samples were measured using a superconducting interference device (SQUID) magnetometer. The magnetization hysteresis

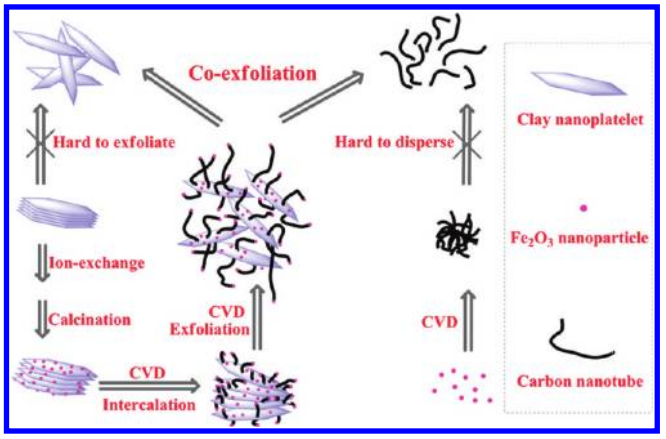

Figure 1. Schematic illustration showing the procedure for the preparation of magnetic CNT−clay hybrids through growth of CNTs within clay nanoplatelet interlayers.

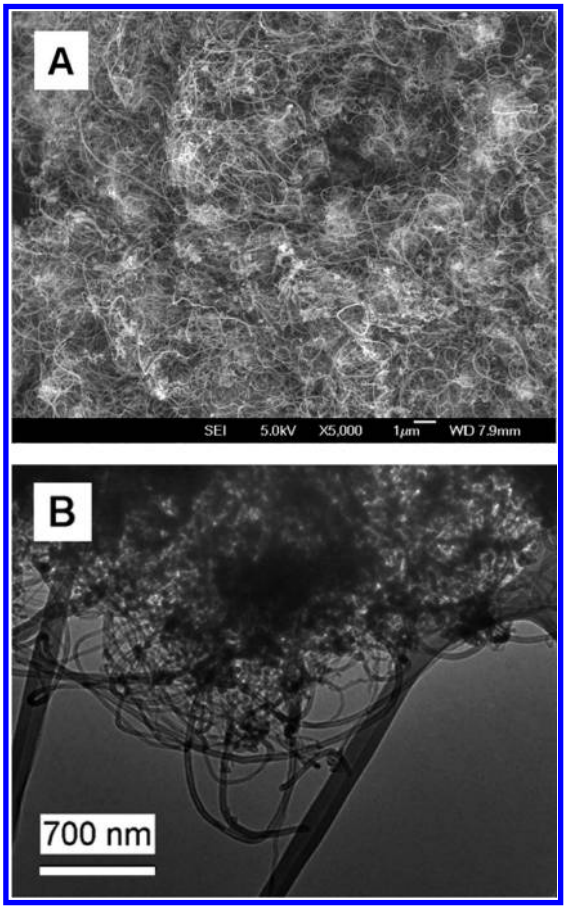

Figure 2. Typical (A) SEM and (B) TEM image showing the CNT−clay hybrids.

loops were measured in fields between ±20 kOe at 300 K, with the fields applied perpendicular to the sample plane.

3. RESULTS AND DISCUSSION

Figure 1 illustrates the procedure for the preparation of magnetic CNT−clay hybrids through CVD growth of CNTs onto clay nanoplatelets. First, the Na^+MMT was modified by

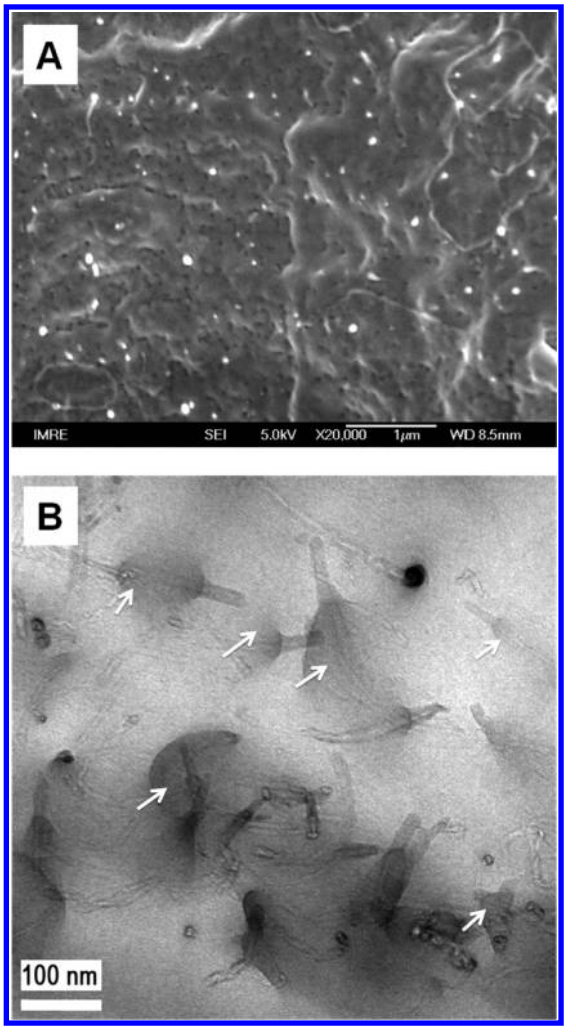

Figure 3. (A) SEM image showing the overall morphology of a quencher cracking surface for the nylon-6 composite with 1 wt % CNT-clay hybrids. (B) TEM image of a thin section of the same sample.

ion-exchange with a $Fe(NO_3)_3$ solution, and thus Fe^{3+} ions were intercalated within the interlayers of MMT. Calcination was then used to change Fe^{3+} ions into Fe_2O_3 particles. During CVD growth of CNTs, the Fe_2O_3 nanoparticles act as seeds or nuclei for the growth of CNTs. The platelets of the clay were further delaminated and exfoliated during the CNT growth within their interlayers, thus forming 3D heterostructures containing 2D clay nanoplatelets surrounded with some CNTs. Typically, the pristine clay minerals cannot be easily exfoliated in water or other solvents, so are the CNTs prepared by CVD methods without modifications. Therefore, a coexfoliation (of CNTs and clay) could be achieved by the direct CVD growth of the CNTs within the galleries of clay nanoplatelets. Moreover, we assume that the obtained CNT−clay hybrids would show excellent mechanical, electrical, and magnetic properties by optimizing CNT−clay−Fe_2O_3 combinations and their synergistic functions.

Figure 2A presents a typical SEM image of the as-prepared CNT−clay hybrid sample. CNTs grow out from the clay platelets, forming a hybrid of clay nanoplatelets combining with CNTs. It can be seen that the CNTs are randomly and loosely entangled. Aggregation of clay particles is not observable under low magnifications. The morphology and structure of the

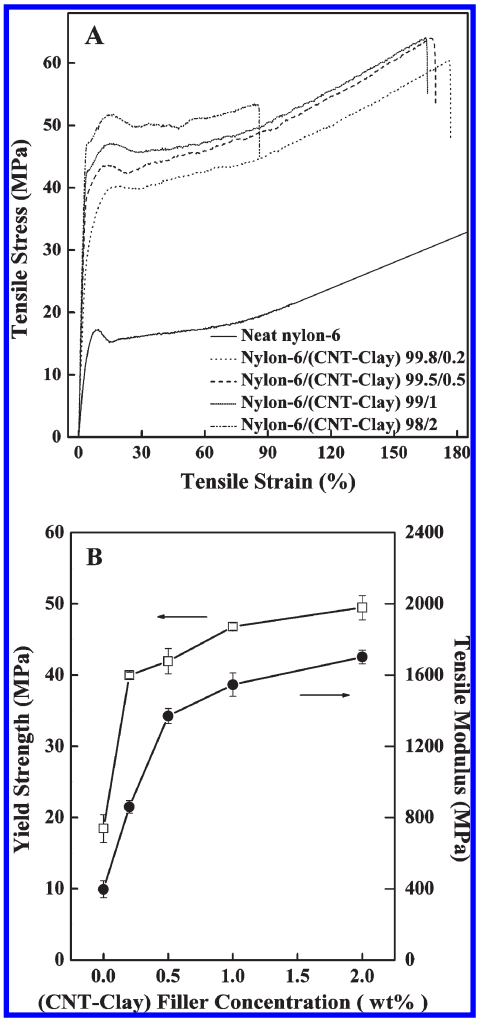

Figure 4. (A) Typical stress−strain curves of neat nylon-6 and its CNT−clay hybrid composites at a crosshead speed of 5 mm min^{-1}. (B) Yield strength and tensile modulus of nylon-6/(CNT−clay) composites as a function of CNT−clay hybrid loading.

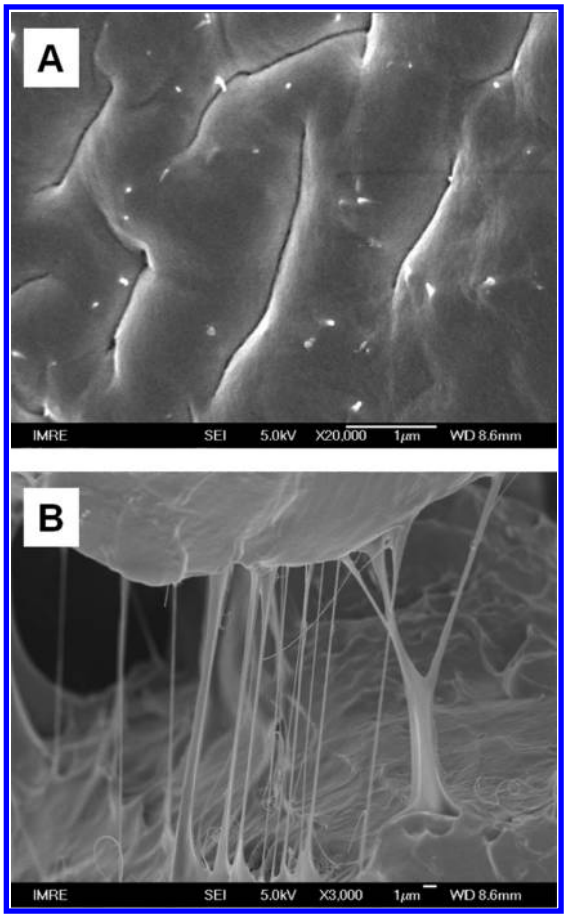

Figure 5. SEM image showing (A) the fracture surfaces of tensile test specimens and (B) the microcrack linked by MWNTs sheathed with polymer in the nylon-6 composite containing 1 wt % CNT−clay hybrid.

CNT−clay hybrid is further observed to obtain more morphology details by TEM, as shown in Figure 2B. One can see that the CNTs are randomly distributed and attached onto the clay particles (dark area in contrast), thus forming a unique structure in which a 2D clay platelet has several 1D CNTs attached to it.

A melt-compounded sample of nylon-6 composite containing 1 wt % CNT-clay hybrid fillers was cryo-fractured in liquid nitrogen, and an overall morphology of the fracture surface is demonstrated in Figure 3A. The uniformly dispersed bright dots are the ends of the broken CNTs, indicating a homogeneous dispersion of the 1D CNTs in the nylon-6 matrix. However, the area containing clay nanoplatelets is not clear only from the evidence provided by the fracture surface by SEM. Therefore, TEM observations of a microtomed thin section of the composite were conducted and are shown in Figure 3B. The dark areas represent the added hybrid fillers, whereas the light areas represent the nylon-6 matrix. One can clearly see that individual CNTs in the tube shape are randomly dispersed within the matrix, and no CNT aggregations are observed. Clay platelets attached to the CNTs are clearly observed, as indicated by the white arrows. Thus, the TEM image clearly exhibits the intimate adhesion of CNTs and clay platelets with the matrix and the combination of CNT−clay hybrid with the polymer matrix. Most interestingly, the residual iron oxide nanoparticles in a sphere shape attached to the end of CNTs are also captured in the TEM image (black dots in Figure 3B).

Typical stress−strain curves of neat nylon-6 and its CNT−clay hybrid composites with different loadings are shown in Figure 4A. It can be concluded that all the specimens have a pronounced yield and postyield drop ascribed to crystallization, showing a linear elastic behavior in low stress region before yielding and a plastic deformation at high stress. As shown in Figure 4B, both the tensile modulus and the yield strength of neat nylon-6 and its nanocomposites increase steadily with increasing hybrid nanofiller loadings. Compared with the neat polymer, the tensile modulus and the yield strength of nylon-6/(CNT−clay) composite systems are significantly improved by about 289% and 154%, respectively, upon adding 1 wt % hybrid nanofillers, while limited improvement of the tensile modulus and yield strength is observed when incorporating even more hybrid nanofillers into the matrix. The elongation at break slightly decreases upon adding 1 wt % hybrid nanofillers, indicating that the composite becomes kind of brittle compared with neat nylon-6. Generally, the remarkable reinforcement of the overall mechanical properties of nylon-6 nanocomposites can be attributed to the fine dispersion of the hybrid nanofillers in the matrix and strong interfacial interactions between the nanofillers and the matrix.

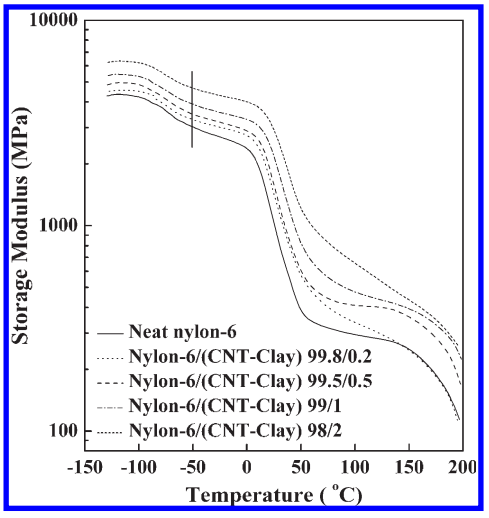

Figure 6. Storage modulus E' versus the temperature curves for nylon-6 and its composites as a function of CNT−clay hybrid loading.

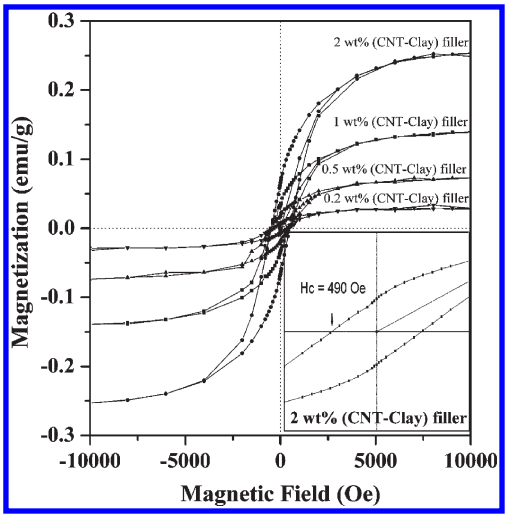

Figure 7. M−H curves of the nylon-6 composite containing different CNT−clay hybrid loadings. For clarity, the inset graph is hysteresis loop between −1000 and 1000 Oe expanded for the nylon-6 composite containing 2 wt % CNT−clay hybrids.

Table 1. DMA, DSC Data and Magnetic Properties of Neat Nylon-6 and Its Nanocomposites Containing Different Loading (wt %) CNT−Clay Hybrid Fillers

nylon-6/(CNT−clay hybrids)	100/0	99.8/0.2	99.5/0.5	99/1	98/2
storage modulus at −50 °C (MPa)	3025	3275	3500	3900	4680
storage modulus at 100 °C (MPa)	295	335	410	475	650
tan (δ)	27.2	29.9	29.9	37.5	44.4
T_m (°C)	220.9	221.2	221.2	221.0	221.2
$T_{c,c}$ (°C)	180.5	194.5	194.6	195.3	195.6
saturated magnetization (emg g^{-1})		0.029	0.073	0.140	0.250
coercive field (Oe)		351	463	500	490

These two factors play key roles in achieving effective load transfer from polymer matrix to nanofillers and leading to the enhanced mechanical properties.

In order to better understand the possible reinforcing mechanisms in the nylon-6/(CNT−clay) composites, the failure surface of the nylon-6 composite containing 1 wt % hybrid fillers upon tensile testing was observed by SEM, as shown in Figure 5. From Figure 5A, it can be seen that the bright dots (i.e., the CNTs) embedded in the nylon-6 matrix are well dispersed. The CNTs are inclined to be broken rather than being pulled out, suggesting a strong filler−polymer interfacial adhesion, thus forming efficient stress transfer from the matrix to the fillers. Interestingly, it can be seen from the crack area that, as shown in Figure 5B, most CNTs or polymer-encapsulated CNTs bridging across the cracks are stretched and well aligned upon tensile testing, which are in favor of the stress release and fracture energy absorption. Therefore, the well dispersed hybrid fillers throughout the polymer matrix and the strong interfacial interaction between fillers and matrix are crucial reasons for the significant reinforcement of the mechanical property of nylon-6 nanocomposites.

Figure 6 shows the dynamic storage modulus versus the temperature curves of nylon-6/(CNT−clay) composites, showing that the storage moduli of the composites steadily increase with the incorporation of hybrid nanofillers especially at high filler loadings. Storage modulus values at −50 and 100 °C from the DMA results for neat nylon-6 and its nanocomposites are summarized in Table 1. The storage modulus of nylon-6 composite containing 2 wt % CNT−clay hybrid nanofillers increases dramatically to 4680 MPa (at −50 °C) in the glassy region, which is 55% larger than that (3024 MPa) of neat nylon-6, indicating that the nanofillers are homogeneously dispersed and have strong interfacial adhesion with the matrix. Overall, the strengthening of storage modulus is more evident at high filler loading, especially higher than 0.5 wt % loading. The maximum of the tan(δ) peak temperature is generally considered as the glass transition temperature (T_g) of the composite. From Table 1, it can be observed that the T_g of the composite is steadily increased by the addition of hybrid nanofillers. This should be explained by the fact that the presence of hybrid fillers in the composite will increase the hindrance of the segmental motion of the nylon-6 chains due to the effects of interfacial interactions and entanglements, thus increasing the T_g of the composites.

The magnetic hysteresis loops for the nylon-6 composites containing different Fe_2O_3 loaded CNT−clay hybrids at room temperature are illustrated in Figure 7. For clarity, the inset is an enlarged hysteresis loop between −1000 and 1000 Oe for the composite containing 2 wt % CNT−clay hybrids. The values of saturation magnetization and coercivity for the nylon-6 composites containing different hybrid nanofiller loadings are summarized in Table 1. The saturation magnetization was observed above ∼15 kOe for all the samples, displaying a ferromagnetic behavior with coercivity ∼430 ± 70 Oe. Both the saturation magnetization and the remanence exhibit a linear relationship with the hybrid nanofiller loading. These observations are in accordance with our expectations, as coercivity is the amount of field required to reduce the remanent magnetization to zero, which is independent of filler loading, whereas both remanence and saturation magnetization are dependent on the amount of magnetic material present in the samples. Since the CNT−clay nanohybrids are directly used without any purification procedures as reinforcing fillers into the nylon matrix, this facile approach to prepare the hybrid nanofillers not only lowers the cost (e.g., avoiding tedious purification), but also endows the fabricated polymer nanocomposites with functional (e.g., magnetic) properties. Therefore, integration of high performance and

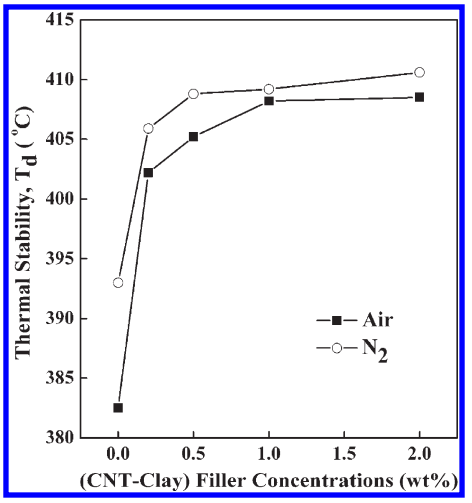

Figure 8. The 5% weight loss temperature versus CNT-clay hybrid content in the air and nitrogen atmospheres summarized by TGA data.

multifunctionality can be achieved simultaneously in the fabricated polymer nanocomposites by using such hybridization and coexfoliation methods.

Thermal stability is one important property for nylon-6 based nanocomposites used as high-performance engineering plastics. Figure 8 presents the thermal decomposition temperatures (at 5% weight loss obtained from TGA measurements in nitrogen and air atmospheres) as a function of hybrid nanofiller loading for neat nylon-6 and its CNT−clay hybrid composites. For the composite with 2 wt % CNT−clay hybrid fillers, the thermal decomposition temperature increases from 393 °C for neat nylon-6 to 411 °C in nitrogen atmosphere, and from 382 °C for neat nylon-6 to 408 °C in air atmosphere, respectively. Therefore, the thermal stability of the composites was significantly improved by the addition of the hybrid nanofillers, which can be attributed to the combined and synergistic effect of the CNT−clay hybrid thermal stability and their strong interfacial interactions with the polymer matrix. It is believed that the formation of compact chars of hybrid nanofillers and polymer matrix during the thermal degradation is beneficial to the improvement of thermal stability of the composites.

WAXD analysis for neat nylon-6 and its composites containing different contents of CNT−clay hybrid was performed at room temperature, and the WAXD patterns are shown in Figure 9A. For neat nylon-6, γ-form crystals (i.e., (001, 200) reflection at 2θ = 21.4°) are apparently observed. With the increase of CNT−clay hybrid filler loadings, reflections at 2θ = 20° and 23.7° corresponding to (200) and (002, 220), respectively, for the α-form crystals of nylon-6, become increasingly clear, showing that the α-form crystals gradually become the dominant phase. From the WAXD curves shown in Figure 9B, crystallization of nylon-6 induced by different kinds of nanofillers, such as CNTs, clay and CNT−clay hybrids was studied and compared. As reported previously in the literature for nylon-6/CNT composites.[29,35] CNTs, acting as nucleation sites, play a role in the formation of thermodynamically stable α-phase crystals of nylon-6. However, the formation of γ-form crystals was strongly enhanced by the presence of clay, that is, an $\alpha \rightarrow \gamma$ crystal transformation always occurs upon adding clay into the nylon-6 matrix. From Figure 9B, the nucleation sites provided by the heterostructured hybrids seem to be favorable to the

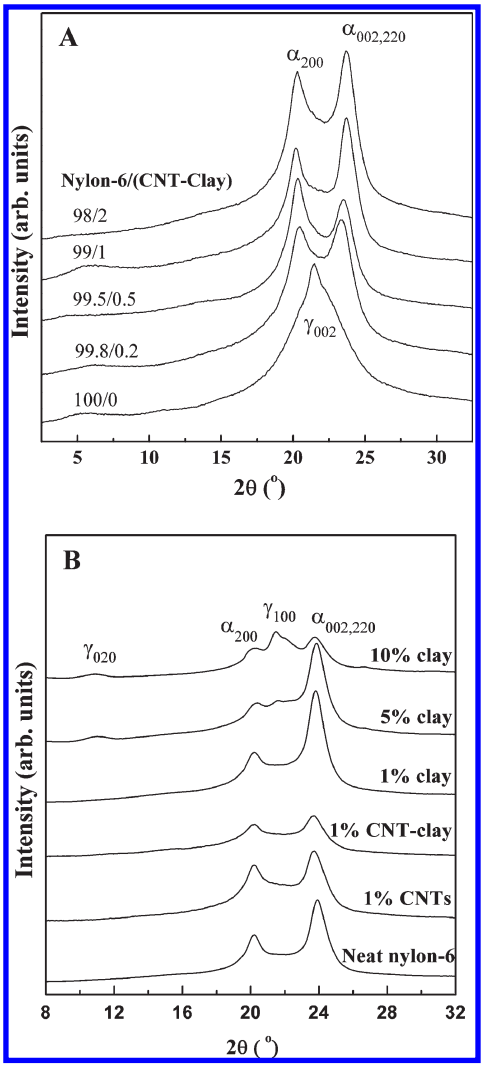

Figure 9. (A) XRD patterns for neat nylon-6 and its composites as a function of CNT−clay hybrid content. (B) XRD patterns for neat nylon-6 and its composites containing clay, CNTs, and CNT−clay hybrid fillers. All the samples have the same thermal history before characterization.

formation of thermodynamically stable α-phase crystals of nylon-6, indicating that within the CNT−clay hybrid nanostructures, the nucleation role of nanoclay to form unstable γ-crystals is greatly inhibited by the CNTs grown on the clay nanoplatelets. This is further supported by the differential scanning calorimetry (DSC) results, as shown later.

It is crucial to study the crystallization and melting behavior of neat nylon-6 and its nanocomposites because crystal structures and crystallinity play significant roles in the mechanical and other properties of crystalline polymers. Figure 10A,B show the DSC heating and cooling curves, respectively, for nylon-6 composites as a function of CNT−clay hybrid nanofiller concentration. For Figure 10A, in comparison with neat nylon-6, the melting point, T_m (~221 °C) as shown in Table 1, is not much affected by the addition of hybrid fillers. There exists a well-developed "cold-crystallization" peak at 65.4 °C for neat nylon-6, indicating that some uncrystallized amorphous phase may have experienced a reorganization or recrystallization process upon heating. For nylon-6 composites containing CNT−clay hybrids, upon

dx.doi.org/10.1021/jp112284k |J. Phys. Chem. B 2011, 115, 3392–3399

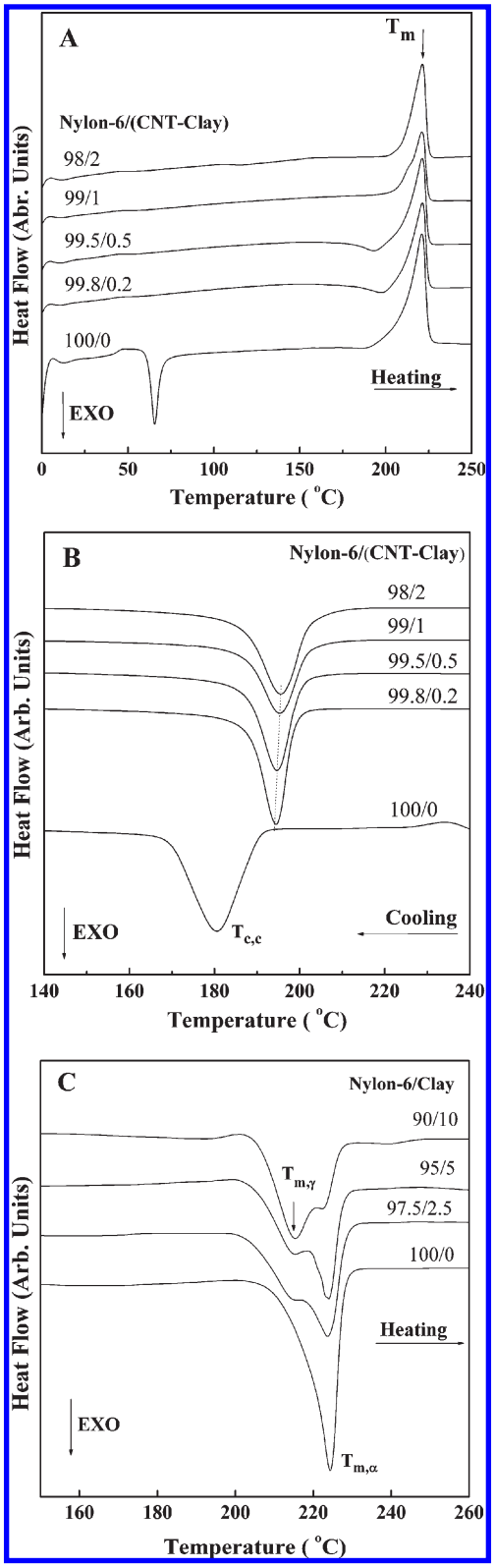

Figure 10. DSC (A) heating and (B) cooling curves for neat nylon-6 and its CNT−clay composite samples. (C) DSC heating curve for neat nylon-6 and clay nanocomposite samples. All the samples have the same thermal history before characterization.

heating from the glassy state, the temperature for the hybrid filler-induced crystallization decreases with the increase of hybrid nanofillers, because the hybrid fillers acted as heterogeneous nucleation sites, thus promoting the crystallization rate and lowering the degree of crystallinity in the nanocomposites. The melt crystallization temperature ($T_{c,c}$) of neat nylon-6 and its composites can be determined when cooling the samples from the molten state in DSC. For Figure 10B, the $T_{c,c}$ of nylon-6/(CNT−clay) composites was increased to be around 195 °C, compared with that (180.5 °C) of neat nylon-6, indicating that the hybrid nanostructures act as heterogeneous nucleating agents. In addition, the melting peaks of the nylon-6 nanocomposites are narrower than in neat nylon-6, suggesting a narrower crystallite size distribution in the nanocomposites. Figure 10C shows the DSC heating curves of neat nylon-6 and its nanocomposites as a function of clay concentration. Upon heating, only one endothermic peak ($T_{m,\alpha}$), ascribing to the melting of α-form crystals of nylon-6, was observed at 225 °C for neat nylon-6, indicating that the α-crystals are the dominant crystalline phase. After incorporation with clay, one can see that another endothermic peak ($T_{m,\gamma}$), corresponding to the melting of the less stable γ-form crystals of nylon-6, was observed at around 215 °C as a shoulder of $T_{m,\alpha}$. With increasing the clay content, the melting peak of γ-form crystals gradually becomes evident and dominant. Therefore, the addition of clay greatly promotes the phase transformation from the α-crystals to the γ-crystals, which is usually not desirable in practice due to the poorer mechanical properties of the γ-crystals compared with those of the α-crystals, as clearly documented by nanoindentation in our previous work.[36] Hence, we believe that the heterogeneous nucleation and formation of the dominant α-crystals induced by the addition of CNT−clay hybrid nanofillers will also play a role in the enhancement of the mechanical performance of nylon-6 nanocomposites fabricated here.

4. CONCLUSIONS

In summary, the CNTs have been grown via direct iron-catalyzed CVD on clay nanoplatelets as catalyst carriers, thus carrying out in situ intercalation and exfoliation of clay nanoplatelets to form nanostructured 1D CNT−2D clay nanoplatelet heterostructures. Without any purification, the CNT−clay hybrids were directly used to fabricate nylon-6 nanocomposites via simple melt-compounding. Simultaneously, the usually considered impurities (i.e., residual iron oxide nanoparticles) endowed the fabricated polymer nanocomposites with functional (e.g., magnetic) properties. By using such hybridization and coexfoliation methods, nylon-6 nanocomposites reinforced with different loadings of the as-prepared CNT−clay hybrid nanofillers showed remarkable enhancement in mechanical properties due to the homogeneous dispersion of nanohybrids and their strong interfacial interaction with the nylon matrix. In addition to these, the nucleation sites provided by the heterostructured hybrids were favorable to form thermodynamically stable α-phase crystals of nylon-6, thus resulting in the successful fabrication of high performance and functional nylon-6-based nanocomposites.

■ AUTHOR INFORMATION

Corresponding Author

*E-mail: txliu@fudan.edu.cn (T.L.); zhangwd@scut.edu.cn (W.Z.).

■ ACKNOWLEDGMENT

The authors are grateful for the financial support from the National Natural Science Foundation of China (20774019;

50873027) and the "Shu Guang" project (09SG02) supported by the Shanghai Municipal Education Commission and the Shanghai Education Development Foundation.

REFERENCES

(1) Henglein, A. *Chem. Rev.* **1989**, *89*, 1861.
(2) Link, S.; El-Sayed, M. A. *Int. Rev. Phys. Chem.* **2000**, *19*, 409.
(3) Trindade, T.; O'Brien, P.; Pickett, N. L. *Chem. Mater.* **2001**, *13*, 3843.
(4) Wang, Z. L. *Annu. Rev. Phys. Chem.* **2004**, *55*, 159.
(5) Kulzer, F.; Orrit, M. *Annu. Rev. Phys. Chem.* **2004**, *55*, 585.
(6) Chujo, Y.; Saegusa, T. *Adv. Polym. Sci.* **1992**, *100*, 11.
(7) Novak, B. M. *Adv. Mater.* **1993**, *5*, 422.
(8) Schubert, U.; Husing, N.; Lorenz, A. *Chem. Mater.* **1995**, *7*, 2010.
(9) Loy, D. A.; Shea, K. J. *Chem. Rev.* **1995**, *95*, 1431.
(10) Judenstein, P.; Sanchez, C. *J. Mater. Chem.* **1996**, *6*, 511.
(11) Sanchez, C.; Soler-Illia, G. J.; Ribot, F.; Lalot, T.; Mayer, C. R.; Cabuil, V. *Chem. Mater.* **2001**, *13*, 3061.
(12) Baughman, R. H.; Zakhidov, A. A.; de Heer, W. A. *Science* **2002**, *297*, 787.
(13) Dai, H. *Acc. Chem. Res.* **2002**, *35*, 1035.
(14) Sun, Y. P.; Fu, K.; Lin, Y.; Huang, W. *Acc. Chem. Res.* **2002**, *35*, 1096.
(15) Kovtyukhova, N. I.; Mallouk, T. E.; Pan, L.; Dickey, E. C. *J. Am. Chem. Soc.* **2003**, *125*, 9761.
(16) Iijima, S. *Nature* **1991**, *354*, 56.
(17) Popov, V. N. *Mater. Sci. Eng.* **2004**, *43*, 61.
(18) Zhang, W. D.; Phang, I. Y.; Liu, T. X. *Adv. Mater.* **2006**, *18*, 73.
(19) Dubois, P.; Alexandre, M. *Adv. Eng. Mater.* **2006**, *8*, 147.
(20) Liu, L.; Grunlan, J. C. *Adv. Funct. Mater.* **2007**, *17*, 2343.
(21) Zhang, Q.; Zhao, M. Q.; Liu, Y.; Cao, A. Y.; Qian, W. Z.; Lu, Y. F.; Wei, F. *Adv. Mater.* **2009**, *21*, 2876.
(22) Sun, D.; Chu, C. C.; Sue, H. J. *Chem. Mater.* **2010**, *22*, 3773.
(23) Zhao, M. Q.; Zhang, Q.; Jia, X. L.; Huang, J. Q.; Zhang, Y. H.; Wei, F. *Adv. Funct. Mater.* **2010**, *20*, 677.
(24) Zhang, C.; Ren, L. L.; Wang, X. Y.; Liu, T. X. *J. Phys. Chem. C* **2010**, *114*, 11435.
(25) Tian, L.; Meziani, M. J.; Lu, F.; Kong, C. Y.; Cao, L.; Thome, T. J.; Sun, Y.-P. *ACS Appl. Mater. Interfaces* **2010**, *2*, 3217.
(26) Fan, H. Y. *Chem. Commun.* **2008**, *12*, 1383–1394.
(27) Andrews, R.; Weisenberger, M. C. *Curr. Opin. Solid State Mater. Sci.* **2004**, *8*, 31.
(28) Xia, H.; Wang, Q.; Qiu, G. *Chem. Mater.* **2003**, *15*, 3879.
(29) Liu, T. X.; Phang, I. Y.; Shen, L.; Chow, S. Y.; Zhang, W. D. *Macromolecules* **2004**, *37*, 7214.
(30) Lincoln, D. M.; Vaia, R. A.; Wang, Z. G.; Hsiao, B. S. *Polymer* **2001**, *42*, 1621.
(31) Medellin-Rodriguez, F. J.; Burger, C.; Hsiao, B. S.; Chu, B.; Vaia, R. A.; Phillips, S. *Polymer* **2001**, *42*, 9015.
(32) Lincoln, D. M.; Vaia, R. A.; Wang, Z. G.; Hsiao, B. S.; Krishnamoorti, R. *Polymer* **2001**, *42*, 9975.
(33) Liu, T. X.; Tjiu, W. C.; He, C. B.; Na, S. S.; Chung, T. S. *Polym. Int.* **2004**, *53*, 392.
(34) Liu, T. X.; Liu, Z. H.; Ma, K. X.; Shen, L.; Zeng, K. Y.; He, C. B. *Compos. Sci. Technol.* **2003**, *63*, 331.
(35) Brosse, A. C.; Tence-Girault, S.; Piccione, P. M.; Leibler, L. *Polymer* **2008**, *49*, 4680.
(36) Shen, L.; Phang, Y. I.; Liu, T. X. *Polym. Test.* **2006**, *25*, 249.